Supplementary Information (SI) for Energy & Environmental Science.
This journal is © The Royal Society of Chemistry 2026

Supporting Information

Membrane-free osmotic power generators with high-performance energy conversion

Shengyang Zhou,[1†] Dehua Huang,[2,3†] Guangpeng Ma,[1] Xuanyi Tong,[1] Yang Liu,[2,3] Linsen Yang,[2] Tianchi Liu,[2] Xiang-Yu Kong[2,3,4,5]* and Liping Wen[2,3,4,5]**

Experimental Section

Materials and Reagents: 4,4'-Diamino-[1,1′-biphenyl]-2,2'-disulfonic acid (DSA) was prepared according to the previous work. 2,4,6-Triformylphloroglucinol (Tp) was purchased from Jilin Chinese Academy of Sciences-Yanshen Technology Co., Ltd. without further purification. Chitosan quaternary ammonium salt (QC) was from Macklin, and other chemicals were purchased from domestic chemical suppliers and used as received.

Characterizations: ^{13}C-solid state nuclear magnetic resonance (NMR) spectra was recorded on a Bruker AVANCE III spectrometer (100 MHZ, German). Fourier transform infrared (FT-IR) spectra were obtained from Excalibur 3100 (Varian, USA) Fourier transform spectrophotometer to observe the presence of functional groups. The wavenumber range of spectra in absorbance mode was from 4000 to 400 cm^{-1}. X-ray diffraction (XRD) pattern was carried out on a Bruker D8 Focus Powder diffractometer with a Cu Kα radiation source (λ = 0.154 nm), and all experimental data was recorded at the range of 2θ = 5-40 °C. The surface roughness and mechanical strength of SPI/QC bilayers were measured by Atomic Force Microscope (AFM). AFM images were obtained by using a Bruker Fastscan (Bruker Corporation, German) instrument with nanoindentation mode. X-ray photoelectron spectroscopy (XPS) spectra was collected on an Al Kα source (ESCALAB 250Xi). The concentration of ion was determined using the Agilent 5800 ICP-OES.

Preparation of sulfonated polyimine (SPI) aqueous solutions. 0.063 g 2,4,6-triformylphloroglucinol and 0.143 g 4,4'-diamino-3,3'-biphenyldisulfonic acid were dispersed into 4 mL dimethyl sulfoxide and stirred without heating for 10 min. Then, 20 mL DI water was added into the reaction system to faciliated dissolution of SPIs in several hours.

Preparation of SPI/QC composite membranes. Polyacrylonitrile (PAN) ultrafiltration membranes with a scale of 10 cm were selected as substrates, whose porous surface were immersed into the SPI aqueous solutions for 3-10 minutes. Subsequently, the extra solutions were removed and the porous surface of PAN ultrafiltration membranes was cleaned for decreasing aggregated SPI droplets. Then, QC aqueous solutions were set on the surface, and kept for at least 1 min. The extra solutions were removed, and the porous surface of PAN ultrafiltration membranes was washed by DI water. Finally, the composite membranes were heated at 60 ^{o}C for 8 min in order for complete solvent evaporation. Moreover, a free-standing SxQy/SPI nanofilm can be obtained by dissolving PAN substrates by DMF."

Electrical Measurements: The electrical measurements were performed using a Keithley 6487 semiconductor picoammeter (Keithley Instruments, Cleveland, OH). SPI and QC aqueous solutions were settled into two reservoirs to fabricate a cell, respectively. The volume of

reservoir is 3 cm^{-3}. A pair of Ag/AgCl salt-bridge electrodes was selected as the working electrodes. For the test of ion conductance, the two reservoirs were doped with symmetric weight of salts. The *I-V* curves were tested and the corresponding conductance according to Ohm's law were calculated. For the test of osmotic energy conversion, the two reservoirs were doped with NaCl to 0.5 M (artificial sea water) and 0.01 M (artificial river water) NaCl solutions. The effective membrane area for energy harvesting was about 0.8 cm^2.

Electrode Calibration: The V_{oc} and I_{sc} was investigated by measuring the *I-V* curves in presence of a transmembrane concentration gradient. The sweeping voltage was from –0.22 V to +0.22 V with a step of 0.02 V. The measured V_{oc} was composed of the E_{diff} and E_{redox}, the relationship could be expressed by the equation as follow

$$E_{diff} = V_{OC} - E_{redox}$$

V_{oc}, E_{redox}, and E_{diff} represent the measured potential, the redox potential generated by the unequal potential drop at the electrode–solution interface, and the diffusion potential contributed by the ion-selective membrane, respectively.

Energy Conversion Efficiency: For a given concentration gradient, the cation transference number (t_+) can be calculated as follows

$$t_+ = \frac{1}{2}\left[\frac{E_{diff}}{\frac{RT}{zF}\ln\left(\frac{\gamma_H c_H}{\gamma_L c_L}\right)} + 1\right]$$

where R, T, F, z, γ, and C refer to the gas constant, temperature, Faraday constant, charge number, activity coefficient of ions, and ion concentration, respectively.

The energy conversion efficiency of the generator was calculated by the equation as follows

$$\eta = \frac{1}{2}(2t_+ - 1)^2$$

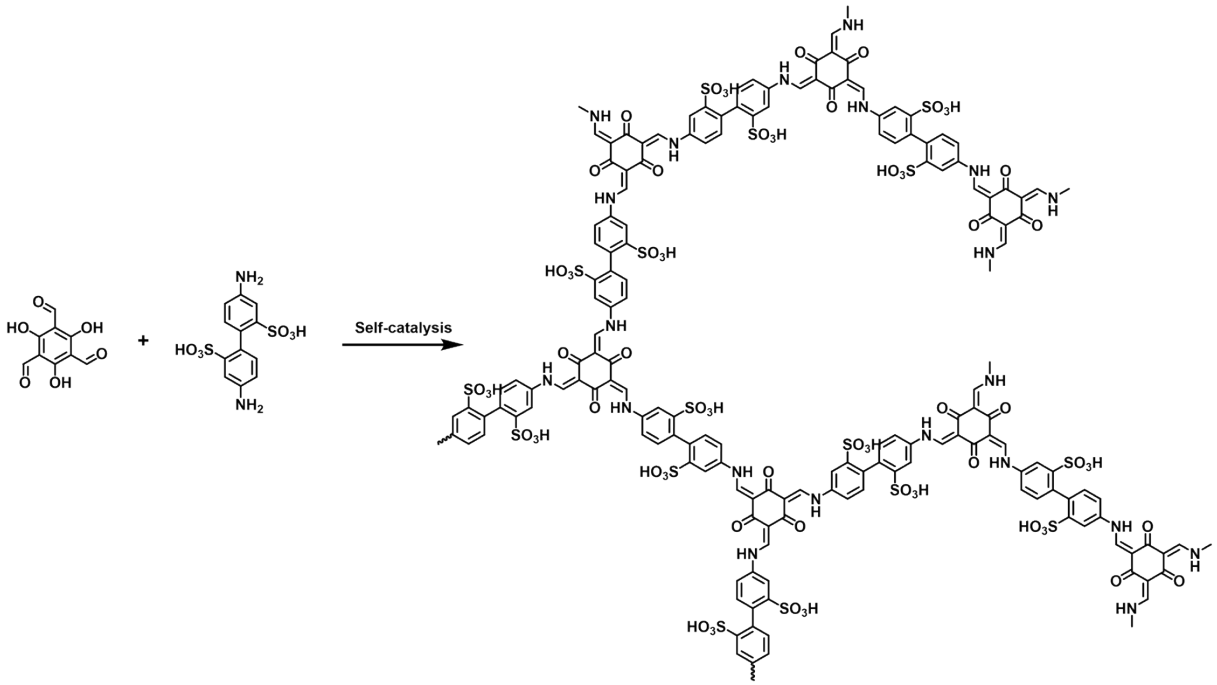

Figure S1. Synthesis of hypercrosslinked sulfonated polyimines (SPIs), using Tp (A_3) and DSA (B_2) as monomers.

Figure S2. Digital photo of SPI aqueous sol with Tyndall effect.

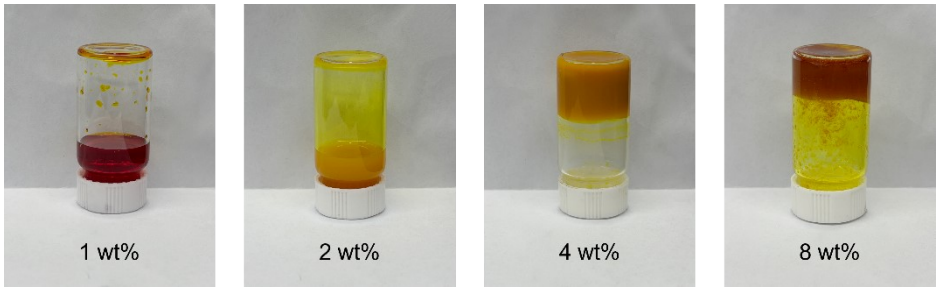

Figure S3. Digital photos of SPI aqueous sols with various concentrations.

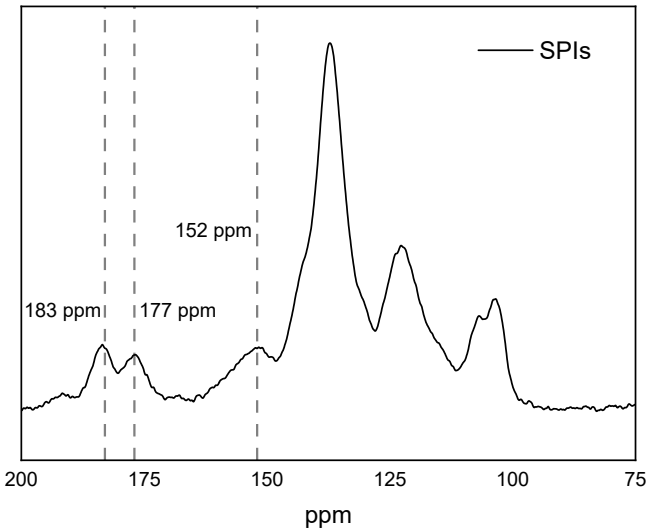

Figure S4. ^{13}C-ssNMR spectra of SPIs. The ^{13}C signals at 152, 177, and 183 ppm belonged to the C=C bonds and C=O bonds, respectively.

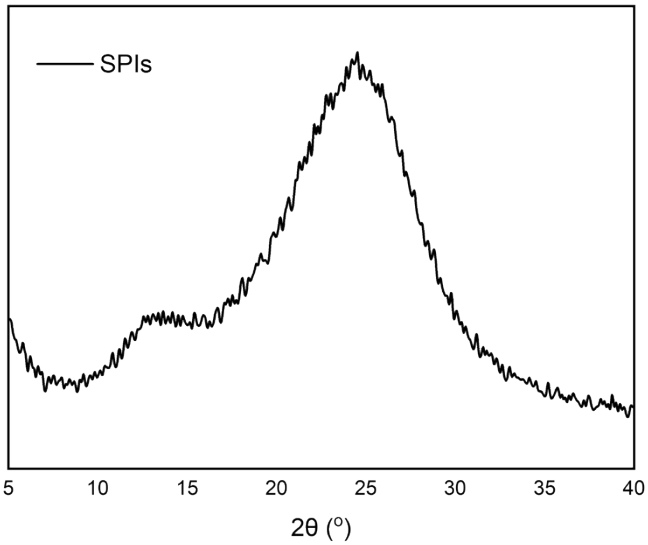

Figure S5. XRD pattern of SPI membranes.

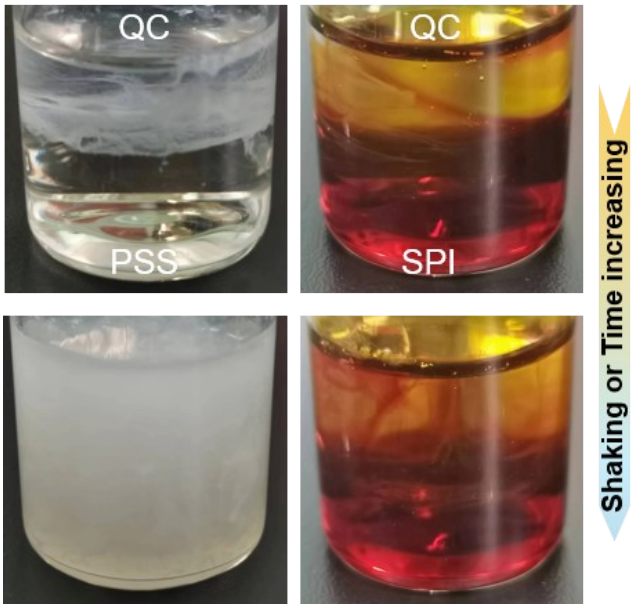

Figure S6. Photographs of mixing polycations and polyanions. Left: polystyrenesulfonate sodium and quaternized chitosans; Right: sulfonated polyimines and quaternized chitosans.

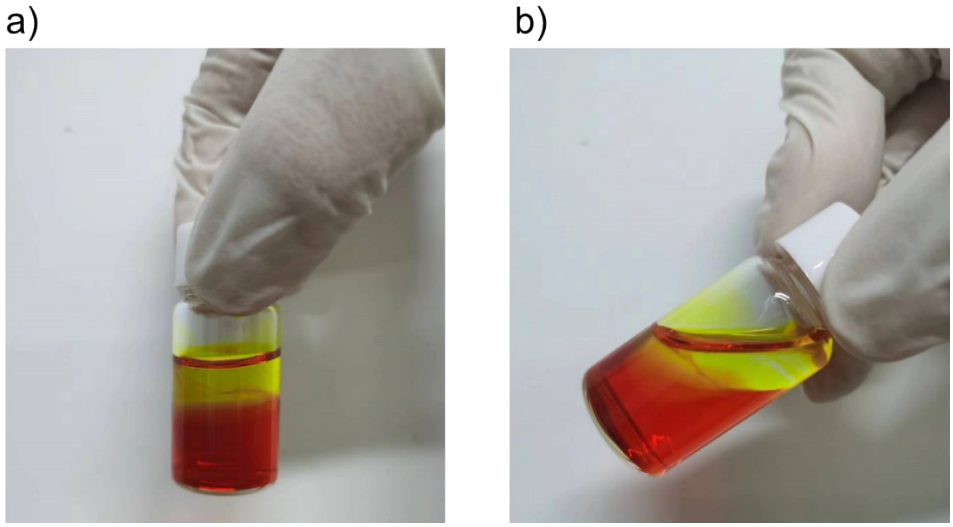

Figure S7. Photographs of SPI/QC ATPS. a) SPI/QC ATPS after 120 h. b) Tilting SPI/QC ATPS after 120 h.

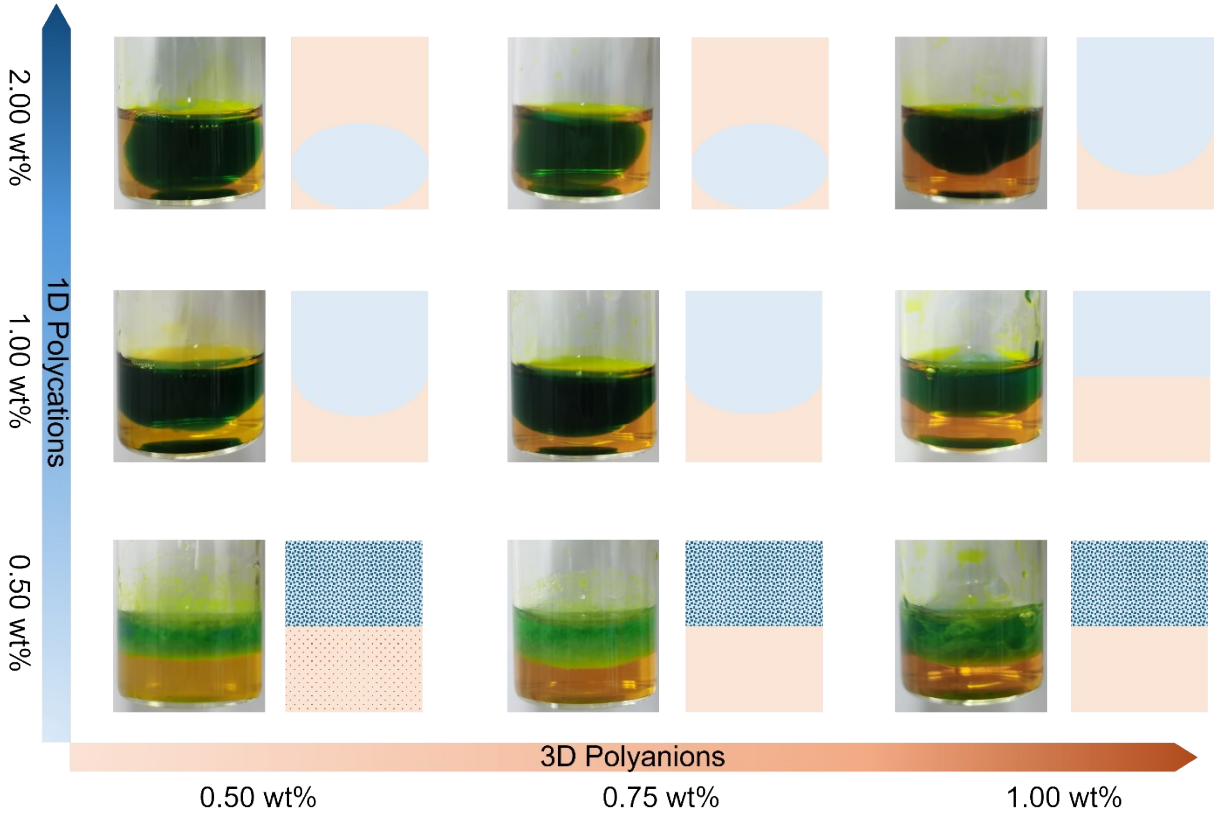

Figure S8. Digital photos of ATPSs of QC aqueous solutions with various concentrations (0.50-2.00 wt%) and SPI aqueous solutions with various concentrations (0.50-1.00 wt%).

Figure S9. Digital photo of ATPS of 1.00 wt% QC and 0.25 wt% SPI aqueous solutions.

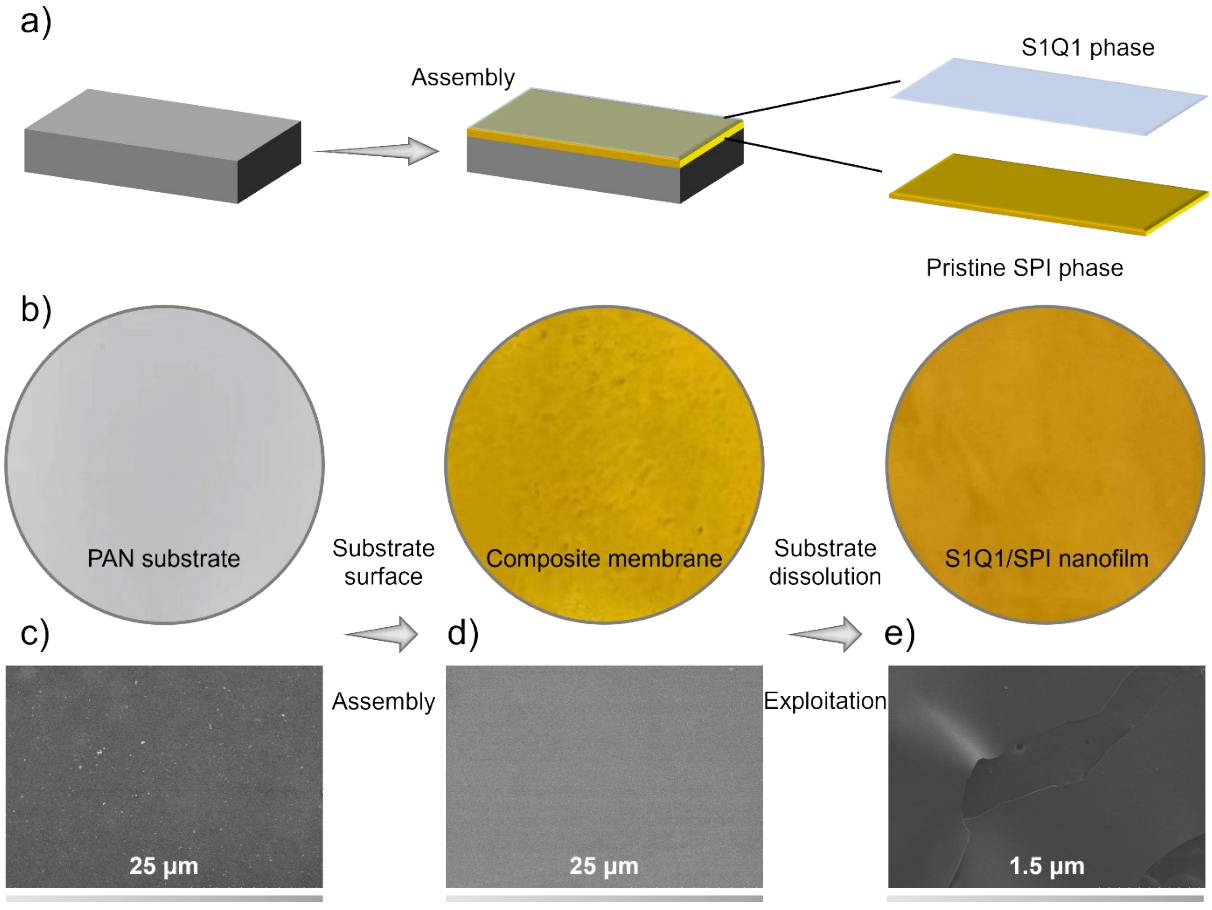

Figure S10. a) Schematic fabrication of SPI/QC-based composite membranes; b) Digital photos of PAN substrates, S1Q1 composite membranes and free-standing S1Q1/SPI nanofilms; c) SEM images of PAN substrates, scale: 25 μm; d) SEM images of S1Q1-based composite membranes, scale: 25 μm; e) SEM images of S1Q1/SPI nanofilms, scale: 1.5 μm.

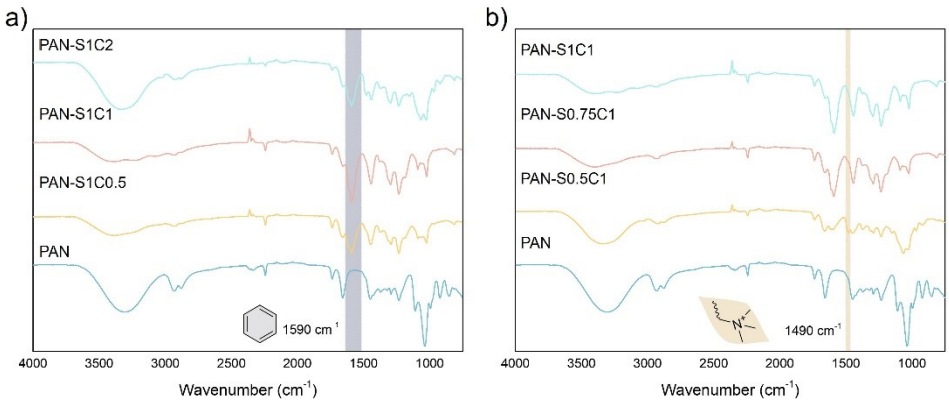

Figure S11. FT-IR spectra of PAN-SxQy membranes. a) Comparison of PAN-S1Qy membranes with PAN substrates. b) Comparison of PAN-SxQ1 membranes with PAN substrates.

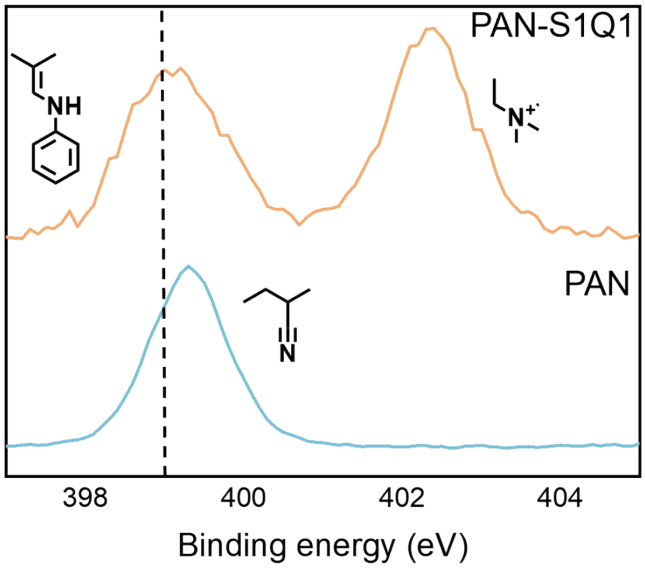

Figure S12. XPS pattern of PAN substrate and PAN-S1Q1 membranes for nitrogen element.

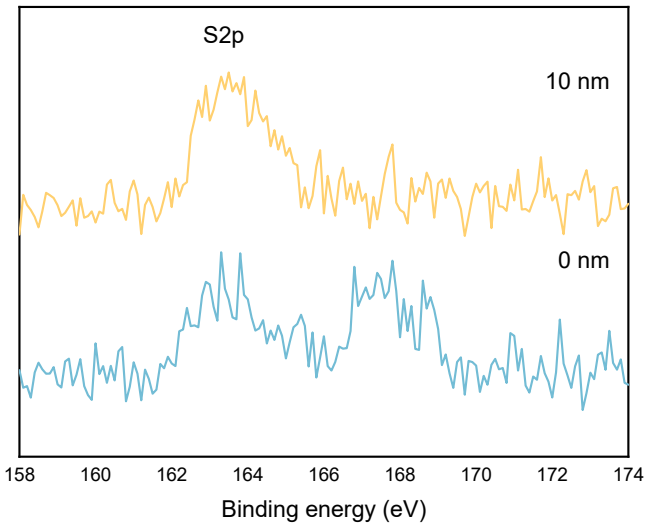

Figure S13. Comparison of S2p binding energy of PAN-S1Q1 membrane, by deep etching 0 nm and 10 nm respectively.

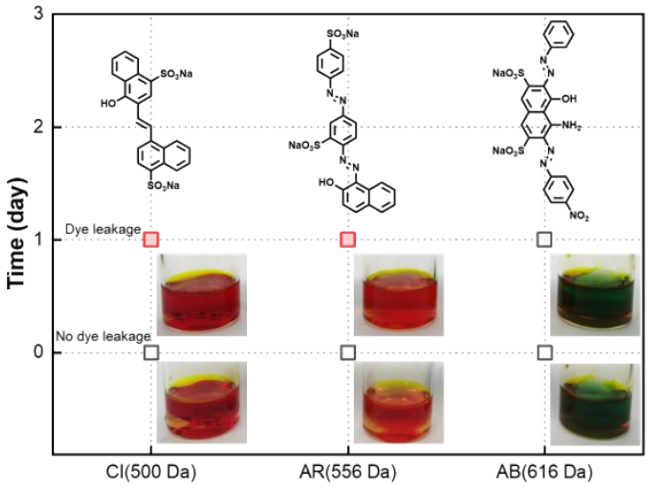

Figure S14. Digital photos of S1Q1 ATPS for dye leakage analysis. QC aqueous solutions were dyed by CI (500 Da), AR (556 Da) and AB (616 Da), respectively.

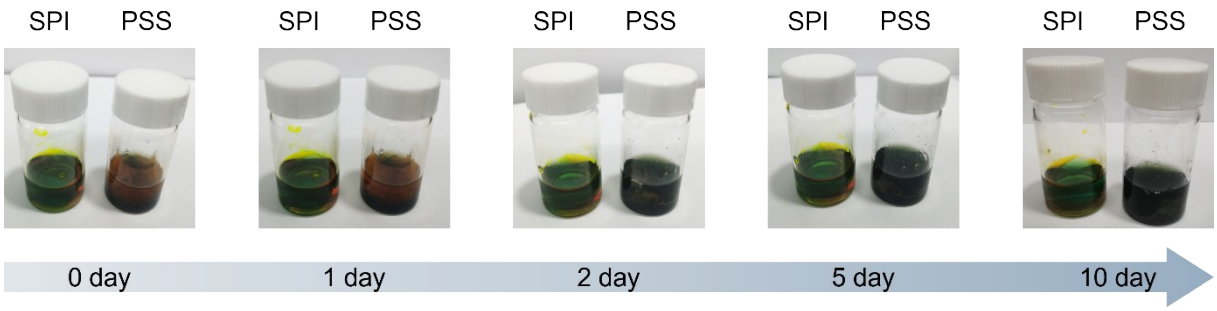

Figure S15. Digital photos of ATPSs of 1.00 wt% QC and 1.00 wt% SPI aqueous solutions, and 1.00 wt% QC and 1.00 wt% PSS aqueous solutions, which maintain different time. QC aqueous solutions were dyed by amino black, and PSS aqueous solutions were dyed by sunset yellow.

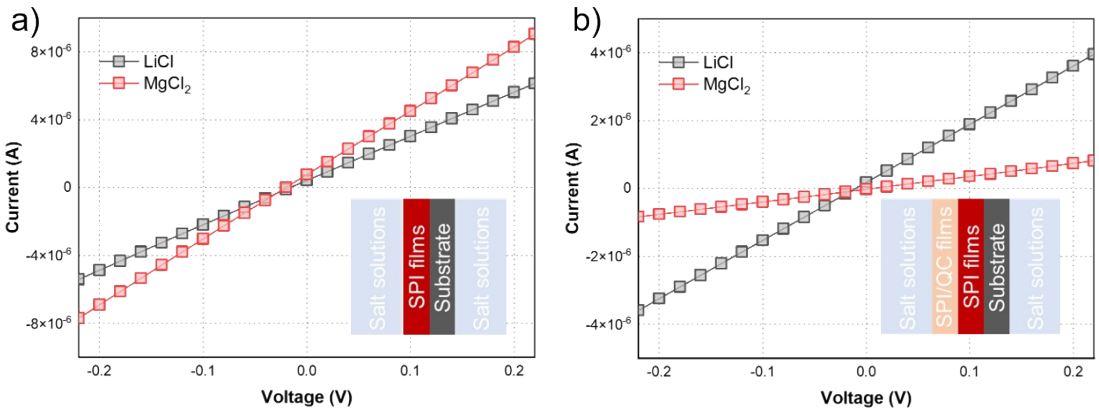

Figure S16. A) *I-V* curves of SPI composite membranes from –0.22 to 0.22 V, using 0.01 M LiCl and $MgCl_2$ aqueous solutions; b) *I-V* curves of S1Q1-based composite membranes from –0.22 to 0.22 V, using 0.01 M LiCl and $MgCl_2$ aqueous solutions.

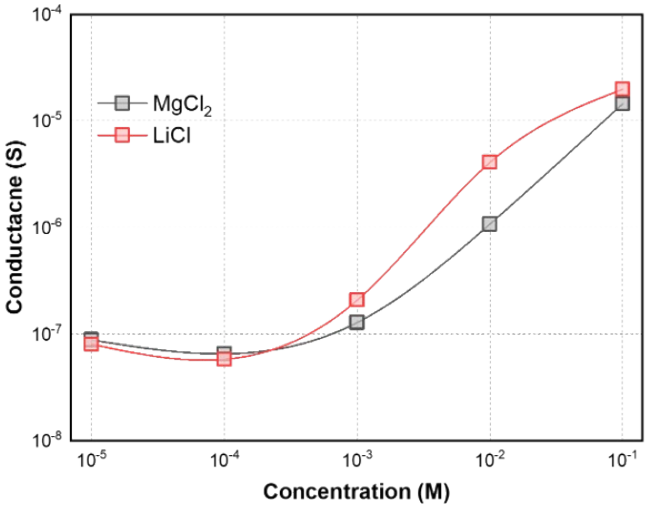

Figure S17. Conductance curves of S1Q1-based composite membranes.

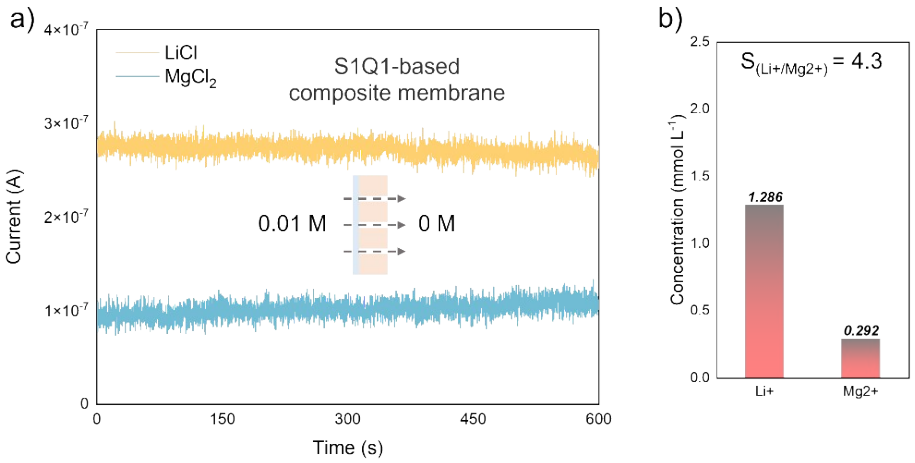

Figure S18. a) *I-T* curves of S1Q1-based composite membranes, respectively using 0.01 M LiCl and $MgCl_2$ aqueous solutions as high-concentration sides and DI water as low-concentration sides; b) Ion diffusion results of S1Q1-based composite membranes, using 0.01 M LiCl and $MgCl_2$ aqueous solutions as high-concentration sides and DI water as low-concentration sides.

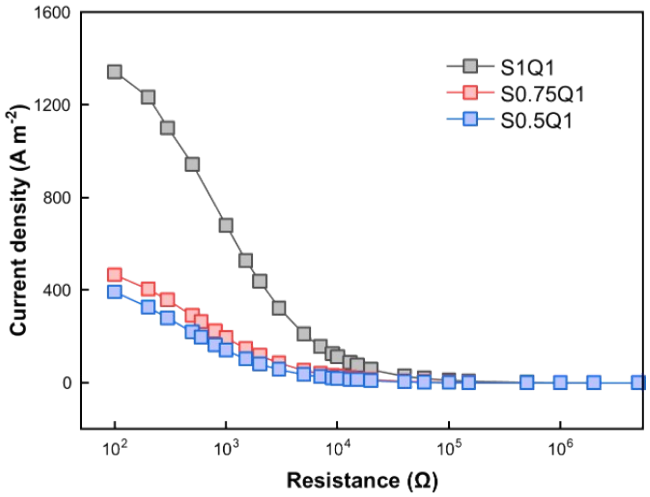

Figure S19. Current density curves of a series of SxQ1-based membrane-free OPGs with a 50-fold NaCl gradient.

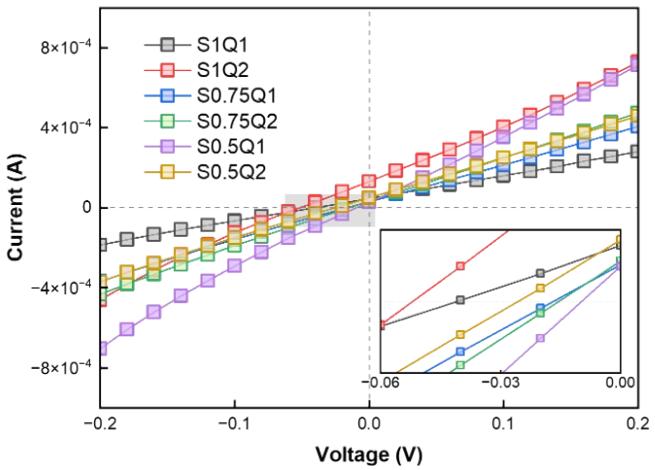

Figure S20. *I-V* curves of SxQy-based membrane-free OPGs with a 50-fold NaCl gradient, from –0.22 to 0.22 V.

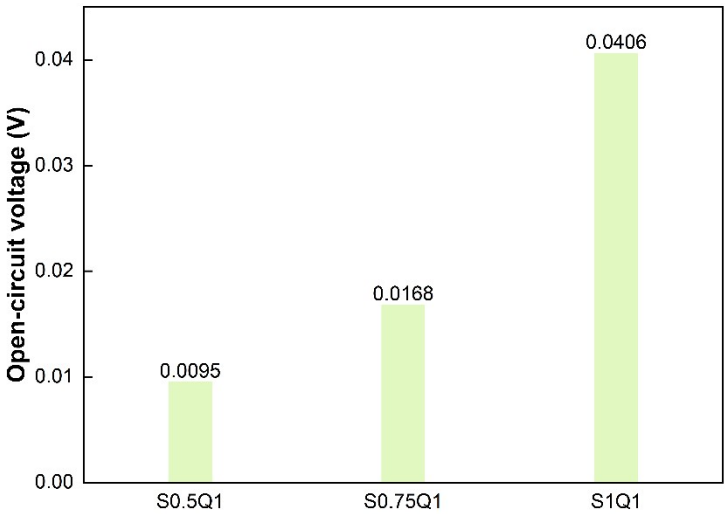

Figure S21. Open-circuit voltage of SxQ1-based membrane-free OPGs under a 50-fold NaCl gradient.

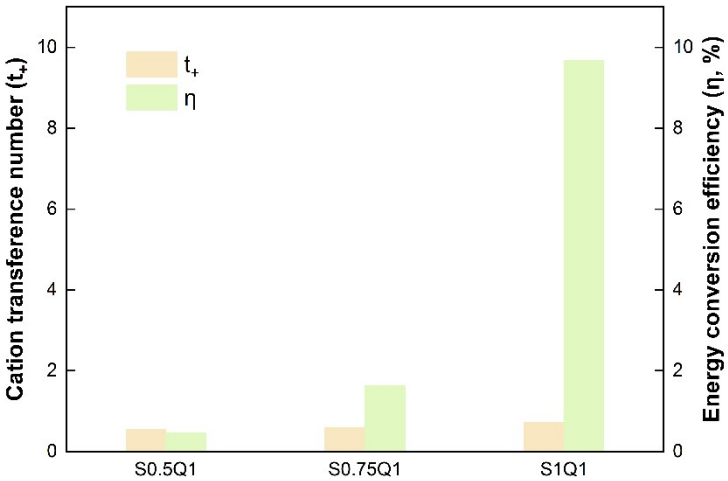

Figure S22. Cation transference number and energy conversion efficiency of SxQ1-based membrane-free OPGs under a 50-fold NaCl gradient.

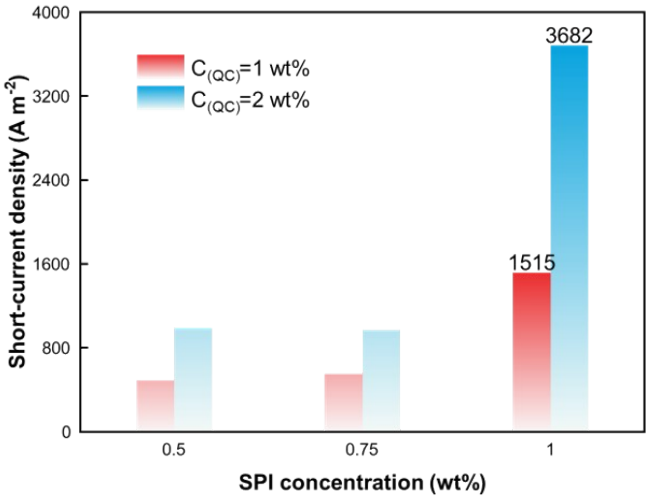

Figure S23. Short-circuit current density of SxQy-based membrane-free OPGs with a 50-fold NaCl gradient.

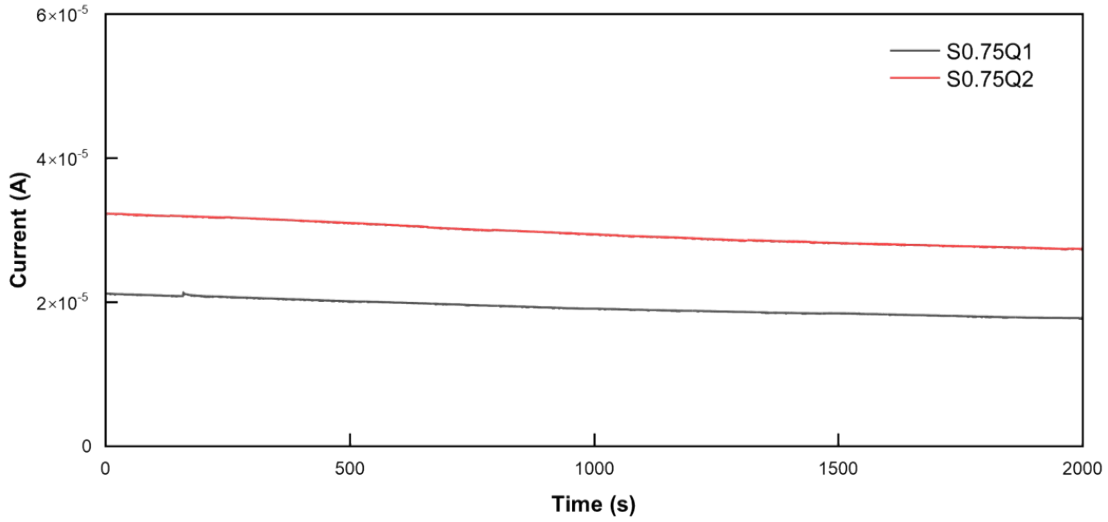

Figure S24. Long-term operation stability of S0.75Qy-based membrane-free OPGs during 2000 s.

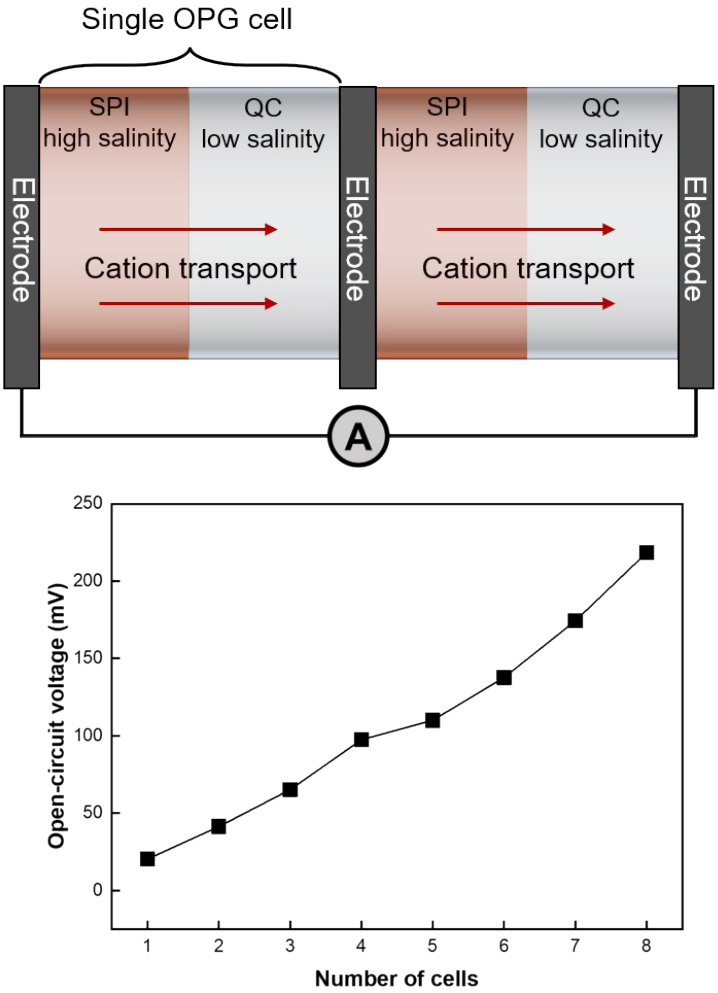

Figure S25. Open-circuit voltage of several S1Q1 droplets coupling in series, using SPI aqueous solutions with high-salinity NaCl and QC aqueous solutions with low-salinity NaCl. Every pair of two droplets can be connected by Ag/AgCl electrodes.

Table S1. Comparison of output power density with reported works on cation-selective membrane-based OPGs at a centimeter scale.

Material	Power density (W m^{-2}) 0.5M/0.01M NaCl	Testing area (m^2)	Reference
BDA-TAM (COF)	2.96	2×10^{-4}	1
Heterolayer gel	17.06 4.52 1.07	7.9×10^{-7} 1.3×10^{-5} 1.1×10^{-4}	2
GDS	1.15 0.65 0.51	$\sim1\times10^{-6}$ $\sim2\times10^{-6}$ $\sim3\times10^{-6}$	3
Ca-COF	24.7	6.36×10^{-8}	4
H-CuMOF-NMs + Commerical AEMs	0.575 (5M/0.01M NaCl)	4×10^{-3}	5
This work	39.42 (Na^+) 74.88 (Cl^-)	8×10^{-5}	-

References

1. C. Wang, J. Tang, L. Li, J. Wan, Y. Ma, Y. Jin, J. Liu, H. Wang and Q. Zhang, *Adv. Funct. Mater.* 2022, **32**, 2204068.
2. W. Chen, K. Zhou, Z. Wu, L. Yang, Y. Xie, X. Meng, Z. Zhao and L. Wen, *J. Am. Chem. Soc.* 2024, **146**, 13191−13200.
3. X. Yang, J. Song, Y. Liu, J. Li, Q. Sun, Z. Liu, J. Tang, Y. Zhang, M. An, H. Liu, Y. Qin and G. Xue, *Adv. Mater.* 2025, **37**, 2505485.
4. W. Jiang, J. Zhou, X. Zhong, M. Fang, J. Hao, D. Zhao, X. Wen, H. Wang, Y. Zhou, Y. Zhu and L. Jiang, *Nat.Sustain.* 2025, **8**, 446–455.
5. K. Li, Z. Yan, S. Yang, W. Xin, X. Li, Y. Wu, K. Zou, D. Huang, H. Ling, T. Liu, Z. Zhang, X.-Y. Kong, L. Jiang and L. Wen, *J. Am. Chem. Soc.* 2025, **147**, 24708−24718.